RAA 2021 Vol. **21** No. **7**, 173(15pp) doi: 10.1088/1674-4527/21/7/173

http://www.raa-journal.org *http://iopscience.iop.org/raa*

***R**esearch in*
***A**stronomy and*
***A**strophysics*

Orbits of 152 globular clusters of the Milky Way galaxy constructed from Gaia DR2

Anisa Talgatovna Bajkova and Vadim Vadimovich Bobylev

Pulkovo Astronomical Observatory, St.Petersburg 196140, Russia; *anisabajkova@mail.ru*

Received 2020 December 10; accepted 2021 March 2

Abstract We present orbits and their properties for 152 globular clusters of the Milky Way galaxy obtained using average Gaia DR2 proper motions and other astrometric data from the list of Vasiliev. For orbital integration we have applied the axisymmetric model of the Galactic potential based on the Navarro-Frenk-White dark halo, and modified by Bajkova & Bobylev utilizing circular velocities of Galactic objects in a wide region of Galactocentric distances (up to 200 kpc) from the Bhattacharjee et al. catalog. Based on the analysis of the obtained orbits, we have modified the composition of the subsystems of globular clusters presented in Massari et al..

Key words: (Galaxy:) globular clusters: general

1 INTRODUCTION

The appearance of accurate astrometric data from measurements from the Gaia satellite of the positions and spatial velocities of globular clusters (GCs, Helmi et al. 2018; Baumgardt et al. 2019; Vasiliev 2019) makes it possible to study their dynamics, origin and evolution (Myeong et al. 2019; Massari et al. 2019; Bajkova et al. 2020).

In this work we present orbits and their properties for almost the entire list of GCs compiled by Vasiliev (2019) on the basis of the most accurate measurements of their velocities and positions to date and implementing one of the best-fit models of the Milky Way gravitational potential. In addition, we set a goal to revise the classification of GCs proposed by Massari et al. (2019) on the basis of analysis of the obtained orbits. In essence, this paper is a supplement to Bajkova et al. (2020), which was devoted to the division of GCs into subsystems of the Galaxy, namely, bulge/bar, thick disk and halo. Recall that in Bajkova et al. (2020) a new criterion for separation of GCs belonging to the disk and halo of the Galaxy was proposed. This criterion is based on the bimodality of the GC distribution L_Z/ecc, where L_Z is the Z component of angular momentum and ecc is eccentricity of the orbit.

In addition to the work of Bajkova et al. (2020), we present here a broader set of orbital parameters, and most importantly, we present a catalog of orbit images in two projections, which enables more fully analyzing them due to visualization. Such work on visualization of the orbits of almost all GCs known to date, and carried out according to the latest data, has been done in the literature for the first time. This work provides, in addition to the available quantitative estimates, the possibility of a qualitative assessment of the GC dynamics, and a comparison of the orbits of different GCs included in different classification groups. In the previous work, we dealt only with the problem of dividing the GCs into those formed in situ and clusters which formed in different progenitors that were only later accreted, i.e. division into disk, bulge and halo subsystems. We did not touch upon the problem of classifying the halo GCs into subsystems, the nature of which is the accretion events of members of other galaxies (the Sausage, Sequoia) onto the Milky Way. An attempt at such a classification was made, for example, in the work of Massari et al. (2019), but we do not consider this work completed, since the analysis of the various diagrams suggests some inconsistencies and contradictions. A qualitative analysis of the orbits allowed us to make some adjustments to Massari et al.'s classification. As a result, we offer our own modified classification, which seems to be more organic. The change in classification affected 27 objects. In addition to the previous article, we present the values of important orbital parameters that were not considered earlier.

This work is structured as follows. Section 2 describes the accepted most realistic model for the axially symmetric Galactic potential. Section 3 is devoted to integrating the orbits and computing parameters of the orbits. Section 4

describes data. In Section 5 we present the catalog of orbits of 152 GCs and their properties. Based on the analysis of the orbits presented, we propose a modified classification of the GCs, which slightly differs from the classification given by Massari et al. (2019). In Conclusions we summarize main results.

2 MODEL FOR THE AXIALLY SYMMETRIC GALACTIC POTENTIAL

In this article the same model of gravitational potential as in Bajkova et al. (2020) is adopted. The axially symmetric gravitational potential of the Galaxy is represented as the sum of three components — the central, spherical bulge $\Phi_b(r(R,Z))$, the disk $\Phi_d(r(R,Z))$ and the massive, spherical dark-matter halo $\Phi_h(r(R,Z))$

$$\Phi(R,Z) = \Phi_b(r(R,Z)) + \Phi_d(r(R,Z)) + \Phi_h(r(R,Z)) \,. \quad (1)$$

Here, we implement a cylindrical coordinate system (R,ψ,Z) with its origin at the Galactic center. In Cartesian coordinates (X,Y,Z) with their origin at the Galactic center, the distance to a star (the spherical radius) is $r^2 = X^2+Y^2+Z^2 = R^2+Z^2$. The gravitational potential is expressed in units of $100\,\mathrm{km}^2\ \mathrm{s}^{-2}$, with distances in kpc, masses in units of the mass of the Galaxy, $M_{\rm gal} = 2.325\times10^7\,M_\odot$, and the gravitational constant is taken to be $G=1$.

We express the potentials of the bulge, $\Phi_b(r(R,Z))$, and disk, $\Phi_d(r(R,Z))$, in the form suggested by Miyamoto & Nagai (1975)

$$\Phi_b(r) = -\frac{M_b}{(r^2+b_b^2)^{1/2}} \,, \quad (2)$$

$$\Phi_d(R,Z) = -\frac{M_d}{\left[R^2+\left(a_d+\sqrt{Z^2+b_d^2}\right)^2\right]^{1/2}} \,, \quad (3)$$

where M_b, M_d are the masses of these components, and b_b, a_d, b_d are the scale parameters of the components in kpc.

For description of the halo component, we referenced the expression in the Navarro-Frenk-White (NFW) form presented in Navarro et al. (1997)

$$\Phi_h(r) = -\frac{M_h}{r}\ln\left(1+\frac{r}{a_h}\right) , \quad (4)$$

where M_h is the mass and a_h is the scale length.

The model of the Galactic potential, considered in this work, is the NFW model modified in Bajkova & Bobylev (2016) by fitting the model parameters to data on HI, maser sources and Galactic objects from Bhattacharjee et al. (2014) at distances R within $\sim$ 200 kpc. In addition the constraints (Irrgang et al. 2013) on the local dynamical matter density $\rho_\odot = 0.1\,M_\odot\ \mathrm{pc}^{-3}$ and the force acting perpendicularly to the Galactic plane $|K_{z=1.1}|/2\pi G = 77 M_\odot\ \mathrm{pc}^{-2}$ were applied.

Note that among six models of the Galactic potential summarized in Bajkova & Bobylev (2017), our model (denoted as Model III in Bajkova & Bobylev (2016, 2017)) ensures the best fit to the data. Here we denote the model as NFWBB for short.

Parameters of the NFWBB model are given in Table 1 of Bajkova et al. (2020). Corresponding rotation curves up to $R = 200$ kpc are displayed in figure 3 of Bajkova & Bobylev (2016). When deriving the model rotation curve, we used $R_\odot = 8.3$ kpc for the Galactocentric distance of the Sun and $V_\odot = 244\ \mathrm{km\ s}^{-1}$ for the linear velocity of the Local Standard of Rest around the center of the Galaxy. The mass of the Galaxy according to this model is $M_{G_{(R\le200kpc)}} = 0.75\pm0.19\times10^{12}\,M_\odot$. This value is consistent with the recently obtained estimate of the lower mass limit for the dark spherical NFW halo $M_{200} = 0.67^{+0.30}_{-0.15}\times10^{12}\,M_\odot$ (Koppelman & Helmi 2020) from the escape velocity utilizing a proper motion selected halo sample.

3 INTEGRATING THE ORBITS AND COMPUTING ORBITAL PARAMETERS

The equation of motion of a test particle in an axially symmetric gravitational potential can be obtained from the Lagrangian of the system $\pounds$ (see Appendix A in Irrgang et al. 2013)

$$\pounds(R,Z,\dot R,\dot\psi,\dot Z) = 0.5(\dot R^2+(R\dot\psi)^2+\dot Z^2) - \Phi(R,Z) \,. \quad (5)$$

Introducing the canonical moments

$$\begin{aligned} p_R &= \partial\pounds/\partial\dot R = \dot R \,, \\ p_\psi &= \partial\pounds/\partial\dot\phi = R^2\dot\psi \,, \\ p_Z &= \partial\pounds/\partial\dot Z = \dot Z \,, \end{aligned} \quad (6)$$

we obtain the Lagrangian equations in the form of a system of six first-order differential equations:

$$\begin{aligned} \dot R &= p_R \,, \\ \dot\psi &= p_\psi/R^2 \,, \\ \dot Z &= p_Z \,, \\ \dot{p_R} &= -\partial\Phi(R,Z)/\partial R + p_\psi^2/R^3 \,, \\ \dot{p_\psi} &= 0 \,, \\ \dot{p_Z} &= -\partial\Phi(R,Z)/\partial Z \,. \end{aligned} \quad (7)$$

We integrated Equation (7) employing a fourth-order Runge-Kutta algorithm.

The Sun's peculiar velocity with respect to the Local Standard of Rest was taken to be $(u_\odot, v_\odot, w_\odot) = (11.1, 12.2, 7.3) \pm (0.7, 0.5, 0.4)$ km s^{-1} (Schonrich et al. 2010). Here, we rely on the heliocentric velocities in a moving Cartesian coordinate system with u directed towards the Galactic center, v in the direction of Galactic rotation, and w perpendicular to the Galactic plane and directed towards the north Galactic pole.

Let the initial positions and space velocities of a test particle in the heliocentric coordinate system be $(x_o, y_o, z_o, u_o, v_o, w_o)$. The initial positions (X, Y, Z) and velocities (U, V, W) of the test particle in Galactic Cartesian coordinates are then given by the formulas:

$$\begin{aligned} &X = R_\odot - x_o, Y = y_o, Z = z_o + h_\odot\,,\\ &R = \sqrt{X^2 + Y^2}\,,\\ &U = u_o + u_\odot\,,\\ &V = v_o + v_\odot + V_\odot\,,\\ &W = w_o + w_\odot\,, \end{aligned} \tag{8}$$

where $R_\odot$ and $V_\odot$ are the Galactocentric distance and the linear velocity of the Local Standard of Rest around the Galactic center, $h_\odot = 16$ pc (Bobylev & Bajkova 2016) is the height of the Sun above the Galactic plane, and Π and Θ are radial and tangential (rotational) velocities respectively.

Below we present the following orbital parameters of GCs:
(1) initial distance of the GC from the Galactic center d_{GC}:

$$d_{GC} = \sqrt{X^2 + Y^2 + Z^2}; \tag{9}$$

(2) radial velocity Π:

$$\Pi = -U\frac{X}{R} + V\frac{Y}{R}; \tag{10}$$

(3) tangential velocity Θ:

$$\Theta = U\frac{Y}{R} + V\frac{X}{R}; \tag{11}$$

(4) total 3D velocity $V_{\rm tot}$:

$$V_{\rm tot} = \sqrt{\Pi^2 + \Theta^2 + W^2}; \tag{12}$$

(5) apocentric distance (apo) of the orbit;
(6) pericentric distance ($peri$) of the orbit;
(7) the eccentricity (ecc) of the orbit:

$$ecc = \frac{apo - peri}{apo + peri}; \tag{13}$$

(8) the components of the angular momentum:

$$L_X = Y \times W - Z \times V; \tag{14}$$

$$L_Y = Z \times U - X \times W; \tag{15}$$

$$L_Z = X \times V - Y \times U; \tag{16}$$

(9) inclination of the orbit θ:

$$\theta = \arccos(\frac{L_Z}{L}), \tag{17}$$

where $L = \sqrt{L_X^2 + L_Y^2 + L_Z^2}$;
(10) period of the orbit T_r;
(11) total energy E:

$$E = \Phi(R, Z) + \frac{V_{\rm tot}^2}{2}. \tag{18}$$

4 DATA

In this paper, as the source of data on GCs, the Vasiliev (2019) catalog serves our purpose. It contains average proper motions calculated from data in the Gaia Data Release 2 (DR2) Catalog, line-of-sight velocities, and (α, δ) positions and distances of 150 GCs. We took data for GC Liller 1 from his previous preprint (Vasiliev 2018). For the GC FSR 1758, we referenced data from Villanova et al. (2019).

The initial position and velocity coordinates (the 6D phase space) $(x_o, y_o, z_o, u_o, v_o, w_o)$ were calculated from these data and utilized for integrating the orbits. Uncertainties in the initial coordinates were calculated using Monte-Carlo simulation (1000 iterations) taking into account the measurement errors given in the catalog of Vasiliev (2019). We adopted the uncertainty in the GCs' heliocentric distances d as 7%, which is about 1.5 times larger than the estimate given by Vasiliev (2019).

Actually, Vasiliev (2019) considered distances from the Harris (2010) catalog, where an error of 0.1 in distance modulus is assumed, corresponding to a relative error of 4.6% in the distance, which, according to Vasiliev (2019), is a rather optimistic choice, since for some clusters, as follows from independent literature sources, the variation in several independent distance estimates could exceed 0.1 mag. It should be borne in mind that there is a possibility of additional error due to inhomogeneity in absorption in the Galaxy, but this is unlikely to give a contribution greater than 0.1 mag (color excess error $E(B-V) \sim 0.03$). Hence, the total error (square root of the sum of squares) in the distance modulus is hardly more than 0.15 mag, which corresponds to about 7% uncertainty in the distances.

Even in the case of an estimate of 4.6%, the distance seems to be the largest source of uncertainty for most of the clusters (Vasiliev 2019), and this aspect is even more serious in our case, as the uncertainty in the distances is assumed to be about 1.5 times larger (7%). Therefore, it makes sense to study the effect of distance uncertainties on the values of the clusters' orbital

Table 1 Orbital properties of the GCs. For each GC we quote values derived from orbits integrated for 5 Gyr backward.

Name	d_{GC} (kpc)	Π (km s^{-1})	Θ (km s^{-1})	$V_{\rm tot}$ (km s^{-1})	apo (kpc)	peri (kpc)	ecc	incl. θ (deg)	T_r (Myr)	L_Z (kpc km s^{-1})	E (km^2 s^{-2})
NGC 104	7.6	6^{+5}_{-9}	192^{+8}_{-4}	197^{+7}_{-3}	$7.7^{+0.1}_{-0.1}$	$5.5^{+0.3}_{-0.2}$	$0.16^{+0.02}_{-0.03}$	27^{+2}_{-1}	116	1328	−126 288
NGC 288	12.2	9^{+3}_{-4}	-42^{+28}_{-22}	66^{+16}_{-14}	$12.3^{+0.3}_{-0.4}$	$1.4^{+0.7}_{-0.8}$	$0.80^{+0.11}_{-0.10}$	119^{+7}_{-16}	142	−349	−116 280
NGC 362	9.5	127^{+18}_{-13}	-1^{+12}_{-12}	145^{+16}_{-9}	$12.1^{+0.3}_{-0.6}$	$0.1^{+0.3}_{-0.0}$	$0.99^{+0.00}_{-0.06}$	92^{+22}_{-19}	126	−10	−121 290
Whiting 1	34.7	-208^{+18}_{-14}	109^{+22}_{-16}	235^{+18}_{-17}	$67.0^{+14.3}_{-9.0}$	$20.3^{+3.4}_{-1.3}$	$0.54^{+0.02}_{-0.05}$	67^{+3}_{-2}	1162	2494	−42 265
NGC 1261	18.2	-95^{+11}_{-9}	-19^{+10}_{-9}	119^{+9}_{-8}	$21.1^{+1.4}_{-1.0}$	$0.7^{+0.2}_{-0.2}$	$0.94^{+0.02}_{-0.04}$	121^{+11}_{-16}	244	−249	−91 385
Pal 1	17.4	42^{+6}_{-8}	214^{+3}_{-4}	219^{+3}_{-3}	$19.1^{+0.4}_{-0.9}$	$14.6^{+0.6}_{-0.8}$	$0.13^{+0.03}_{-0.02}$	14^{+1}_{-1}	350	3646	−78 086
E 1	124.7	11^{+75}_{-72}	-144^{+114}_{-88}	174^{+104}_{-45}	$237.9^{+45.2}_{-42.9}$	$104.3^{+30.3}_{-45.9}$	$0.39^{+0.41}_{-0.00}$	127^{+6}_{-28}	5594	−12100	−15 914
Eridanus	95.2	-90^{+27}_{-31}	-28^{+48}_{-27}	163^{+43}_{-16}	$174.5^{+83.6}_{-24.3}$	$12.0^{+73.4}_{-6.2}$	$0.87^{+0.02}_{-0.31}$	113^{+13}_{-37}	3220	−2064	−23 988
Pal 2	35.3	-108^{+5}_{-5}	11^{+22}_{-23}	108^{+8}_{-2}	$41.0^{+2.0}_{-2.2}$	$0.6^{+1.8}_{-0.4}$	$0.97^{+0.02}_{-0.08}$	42^{+70}_{-35}	506	373	−63 896
NGC 1851	16.9	105^{+4}_{-4}	-1^{+5}_{-5}	133^{+4}_{-4}	$20.1^{+0.7}_{-0.2}$	$0.1^{+0.2}_{-0.0}$	$0.99^{+0.00}_{-0.02}$	92^{+9}_{-9}	232	−22	−94 063
NGC 1904	19.0	46^{+8}_{-3}	12^{+12}_{-9}	47^{+9}_{-0}	$19.7^{+0.5}_{-0.9}$	$0.3^{+0.5}_{-0.1}$	$0.97^{+0.01}_{-0.05}$	60^{+27}_{-25}	218	211	−96 192
NGC 2298	16.0	-92^{+6}_{-8}	-32^{+8}_{-10}	125^{+7}_{-8}	$18.0^{+0.7}_{-0.4}$	$1.2^{+0.5}_{-0.4}$	$0.87^{+0.04}_{-0.05}$	118^{+8}_{-5}	208	−500	−98 716
NGC 2419	90.2	-5^{+10}_{-13}	47^{+30}_{-17}	75^{+31}_{-14}	$91.8^{+7.3}_{-6.1}$	$17.3^{+13.3}_{-5.5}$	$0.68^{+0.09}_{-0.18}$	52^{+14}_{-18}	1562	3907	−35 896
Pyxis	41.5	-247^{+9}_{-5}	-29^{+21}_{-10}	311^{+13}_{-10}	$324.2^{+95.8}_{-90.9}$	$41.7^{+4.7}_{-12.8}$	$0.77^{+0.07}_{-0.01}$	98^{+2}_{-6}	7100	−1205	−15 098
NGC 2808	11.3	-157^{+1}_{-2}	41^{+1}_{-7}	165^{+2}_{-1}	$14.4^{+0.7}_{-0.1}$	$1.0^{+0.0}_{-0.1}$	$0.87^{+0.02}_{-0.00}$	10^{+5}_{-0}	158	457	−111 797
E 3	9.3	44^{+11}_{-16}	251^{+13}_{-18}	276^{+14}_{-18}	$13.1^{+1.9}_{-2.0}$	$9.2^{+0.4}_{-0.5}$	$0.18^{+0.06}_{-0.07}$	29^{+1}_{-1}	224	2240	−97 684
Pal 3	95.9	-147^{+47}_{-70}	89^{+79}_{-62}	184^{+81}_{-20}	$173.4^{+77.4}_{-73.9}$	$76.3^{+29.1}_{-13.7}$	$0.39^{+0.38}_{-0.00}$	67^{+15}_{-14}	4524	6495	−20 091
NGC 3201	9.1	-114^{+17}_{-18}	-301^{+9}_{-9}	355^{+12}_{-11}	$26.3^{+3.7}_{-3.0}$	$8.4^{+0.3}_{-0.3}$	$0.52^{+0.05}_{-0.05}$	152^{+1}_{-1}	372	−2728	−75 483
Pal 4	111.4	-25^{+46}_{-67}	-33^{+63}_{-60}	70^{+72}_{-0}	$116.5^{+22.1}_{-8.5}$	$16.3^{+60.0}_{-1.6}$	$0.75^{+0.01}_{-0.49}$	103^{+7}_{-17}	2032	−1394	−31 065
Crater	144.8	-101^{+110}_{-98}	-63^{+105}_{-270}	135^{+249}_{-0}	$156.1^{+97.5}_{-90.0}$	$117.4^{+42.6}_{-18.0}$	$0.14^{+0.73}_{-0.00}$	108^{+25}_{-26}	5082	−6104	−18 859
NGC 4147	21.5	47^{+9}_{-8}	-3^{+12}_{-22}	136^{+5}_{-5}	$26.4^{+0.6}_{-1.9}$	$0.4^{+0.9}_{-0.0}$	$0.97^{+0.00}_{-0.07}$	93^{+20}_{-12}	314	−27	−81 117
NGC 4372	7.3	16^{+11}_{-14}	133^{+6}_{-9}	150^{+6}_{-7}	$7.3^{+0.3}_{-0.2}$	$3.0^{+0.2}_{-0.3}$	$0.42^{+0.04}_{-0.02}$	28^{+3}_{-2}	98	962	−139 570
Rup 106	18.5	-242^{+5}_{-8}	91^{+16}_{-15}	261^{+12}_{-7}	$37.9^{+5.6}_{-5.1}$	$4.7^{+0.9}_{-0.8}$	$0.78^{+0.03}_{-0.03}$	46^{+6}_{-4}	498	1640	−64 986
NGC 4590	10.3	-169^{+7}_{-12}	293^{+6}_{-12}	339^{+4}_{-6}	$29.9^{+1.4}_{-2.4}$	$8.9^{+0.2}_{-0.4}$	$0.54^{+0.02}_{-0.02}$	41^{+2}_{-3}	428	2453	−70 495
NGC 4833	7.2	105^{+12}_{-15}	40^{+12}_{-13}	120^{+12}_{-13}	$8.0^{+0.4}_{-0.3}$	$0.7^{+0.2}_{-0.3}$	$0.83^{+0.07}_{-0.04}$	36^{+13}_{-8}	86	286	−144 428
NGC 5024	18.5	-95^{+7}_{-6}	141^{+8}_{-10}	184^{+8}_{-10}	$22.3^{+2.1}_{-2.0}$	$8.9^{+1.4}_{-1.4}$	$0.43^{+0.03}_{-0.03}$	74^{+2}_{-2}	332	797	−80 241
NGC 5053	17.9	-89^{+5}_{-3}	134^{+5}_{-9}	164^{+4}_{-8}	$18.0^{+1.1}_{-0.6}$	$10.4^{+1.0}_{-1.1}$	$0.27^{+0.04}_{-0.03}$	76^{+1}_{-1}	300	727	−85 221
NGC 5139	6.6	-70^{+7}_{-4}	-72^{+6}_{-7}	128^{+7}_{-9}	$7.4^{+0.1}_{-0.4}$	$1.1^{+0.3}_{-0.1}$	$0.73^{+0.02}_{-0.05}$	137^{+7}_{-5}	80	−462	−147 850
NGC 5272	12.2	-38^{+7}_{-5}	143^{+10}_{-7}	200^{+8}_{-6}	$15.9^{+0.7}_{-0.9}$	$5.2^{+0.4}_{-0.3}$	$0.51^{+0.01}_{-0.03}$	57^{+1}_{-2}	212	994	−98 226
NGC 5286	8.9	-220^{+4}_{-4}	-44^{+14}_{-15}	224^{+3}_{-1}	$13.7^{+1.2}_{-0.7}$	$0.8^{+0.4}_{-0.2}$	$0.89^{+0.02}_{-0.04}$	123^{+10}_{-10}	154	−375	−113 332
NGC 5466	16.4	172^{+17}_{-22}	-141^{+29}_{-17}	317^{+8}_{-17}	$53.7^{+5.7}_{-10.4}$	$5.9^{+0.6}_{-1.1}$	$0.80^{+0.02}_{-0.02}$	108^{+2}_{-2}	750	−820	−52 693
NGC 5634	21.1	-45^{+12}_{-16}	39^{+15}_{-16}	65^{+11}_{-5}	$21.6^{+1.1}_{-1.1}$	$2.1^{+0.9}_{-0.3}$	$0.82^{+0.02}_{-0.06}$	70^{+7}_{-3}	256	346	−89 143
NGC 5694	29.3	-185^{+8}_{-13}	-44^{+18}_{-22}	252^{+12}_{-10}	$70.4^{+10.4}_{-7.8}$	$2.5^{+1.7}_{-1.0}$	$0.93^{+0.03}_{-0.04}$	136^{+10}_{-17}	992	−1019	−45 290
IC 4499	15.6	-245^{+7}_{-4}	-75^{+9}_{-14}	263^{+4}_{-5}	$30.0^{+3.1}_{-2.7}$	$6.5^{+0.8}_{-0.4}$	$0.65^{+0.02}_{-0.05}$	113^{+4}_{-3}	406	−1066	−72 235
NGC 5824	25.7	-41^{+17}_{-20}	105^{+13}_{-24}	215^{+11}_{-14}	$37.4^{+2.6}_{-4.3}$	$14.0^{+1.7}_{-3.6}$	$0.45^{+0.10}_{-0.05}$	58^{+4}_{-2}	598	2393	−59 779
Pal 5	18.4	-54^{+5}_{-6}	160^{+39}_{-43}	169^{+37}_{-38}	$18.9^{+2.4}_{-0.6}$	$10.7^{+4.3}_{-3.6}$	$0.28^{+0.18}_{-0.13}$	66^{+4}_{-4}	308	1260	−83 194
NGC 5897	7.3	88^{+13}_{-26}	97^{+14}_{-23}	159^{+8}_{-19}	$8.7^{+0.6}_{-0.4}$	$1.9^{+0.4}_{-0.5}$	$0.64^{+0.08}_{-0.05}$	61^{+5}_{-5}	106	362	−131 771
NGC 5904	6.3	-290^{+17}_{-15}	126^{+11}_{-14}	365^{+13}_{-14}	$23.3^{+3.9}_{-3.3}$	$2.3^{+0.5}_{-0.3}$	$0.82^{+0.03}_{-0.03}$	72^{+3}_{-3}	286	402	−85 576
NGC 5927	4.7	-39^{+20}_{-23}	233^{+6}_{-11}	236^{+6}_{-9}	$5.2^{+0.3}_{-0.2}$	$4.2^{+0.4}_{-0.5}$	$0.11^{+0.07}_{-0.05}$	9^{+1}_{-1}	82	1077	−148 662
NGC 5946	5.8	35^{+6}_{-18}	25^{+6}_{-15}	116^{+9}_{-9}	$5.9^{+0.6}_{-0.2}$	$0.4^{+0.2}_{-0.2}$	$0.89^{+0.05}_{-0.05}$	77^{+8}_{-3}	66	141	−158 006
ESO 224-8	12.6	-43^{+60}_{-14}	259^{+21}_{-22}	262^{+19}_{-21}	$17.0^{+3.0}_{-2.7}$	$11.9^{+0.9}_{-1.3}$	$0.18^{+0.08}_{-0.07}$	7^{+1}_{-1}	292	3245	−85 205
NGC 5986	4.7	62^{+21}_{-33}	23^{+16}_{-15}	68^{+24}_{-32}	$5.2^{+0.6}_{-0.0}$	$0.2^{+0.2}_{-0.1}$	$0.93^{+0.05}_{-0.08}$	66^{+10}_{-14}	56	94	−168 505
FSR 1716	4.8	87^{+47}_{-44}	228^{+21}_{-15}	281^{+24}_{-10}	$7.0^{+1.4}_{-0.7}$	$3.9^{+0.7}_{-0.7}$	$0.28^{+0.13}_{-0.07}$	31^{+2}_{-3}	106	1089	−137 191
Pal 14	71.4	117^{+25}_{-18}	16^{+16}_{-41}	177^{+29}_{-17}	$133.9^{+31.3}_{-22.5}$	$2.2^{+5.2}_{-0.4}$	$0.97^{+0.00}_{-0.07}$	50^{+63}_{-0}	2202	794	−29 458
BH 184	4.4	40^{+15}_{-21}	121^{+9}_{-11}	156^{+8}_{-9}	$4.7^{+0.4}_{-0.4}$	$1.7^{+0.2}_{-0.3}$	$0.47^{+0.06}_{-0.04}$	36^{+3}_{-3}	58	531	−168 579
NGC 6093	3.7	33^{+12}_{-17}	16^{+9}_{-19}	71^{+9}_{-7}	$4.3^{+0.0}_{-0.9}$	$0.2^{+0.3}_{-0.1}$	$0.93^{+0.05}_{-0.13}$	83^{+8}_{-5}	44	25	−176 933
NGC 6121	6.3	-52^{+2}_{-2}	10^{+18}_{-12}	54^{+7}_{-2}	$6.4^{+0.2}_{-0.1}$	$0.2^{+0.1}_{-0.1}$	$0.94^{+0.04}_{-0.03}$	21^{+82}_{-31}	68	60	−159 021
NGC 6101	11.1	-12^{+29}_{-12}	-314^{+3}_{-2}	370^{+6}_{-4}	$44.2^{+4.1}_{-4.8}$	$10.9^{+0.4}_{-0.9}$	$0.61^{+0.02}_{-0.02}$	143^{+2}_{-2}	658	−3236	−56 722
NGC 6144	2.7	-69^{+90}_{-93}	-196^{+66}_{-15}	213^{+7}_{-3}	$3.2^{+0.6}_{-0.0}$	$2.1^{+0.2}_{-0.3}$	$0.21^{+0.14}_{-0.01}$	114^{+8}_{-9}	40	−239	−172 662
NGC 6139	3.5	-1^{+16}_{-16}	76^{+4}_{-8}	156^{+9}_{-9}	$3.6^{+0.3}_{-0.1}$	$1.1^{+0.2}_{-0.2}$	$0.54^{+0.07}_{-0.03}$	62^{+4}_{-3}	52	248	−176 480
Terzan 3	2.5	-61^{+45}_{-51}	206^{+7}_{-22}	236^{+7}_{-8}	$3.2^{+0.4}_{-0.2}$	$2.2^{+0.1}_{-0.4}$	$0.18^{+0.13}_{-0.03}$	42^{+6}_{-4}	44	440	−175 324
NGC 6171	3.5	-4^{+7}_{-3}	78^{+15}_{-8}	101^{+13}_{-6}	$3.8^{+0.3}_{-0.3}$	$0.6^{+0.3}_{-0.2}$	$0.72^{+0.08}_{-0.11}$	52^{+7}_{-4}	44	191	−178 959
ESO 452-11	2.1	-24^{+11}_{-15}	-13^{+12}_{-11}	107^{+10}_{-2}	$2.9^{+0.4}_{-0.1}$	$0.0^{+0.1}_{-0.0}$	$0.97^{+0.01}_{-0.03}$	101^{+7}_{-10}	26	−16	−202 684
NGC 6205	8.6	20^{+6}_{-4}	-26^{+5}_{-7}	87^{+5}_{-6}	$8.6^{+0.3}_{-0.2}$	$1.0^{+0.2}_{-0.1}$	$0.79^{+0.03}_{-0.03}$	105^{+4}_{-3}	100	−187	−134 416
NGC 6229	29.9	30^{+11}_{-12}	6^{+8}_{-9}	59^{+8}_{-13}	$31.0^{+1.1}_{-1.0}$	$0.5^{+0.6}_{-0.1}$	$0.97^{+0.01}_{-0.04}$	77^{+26}_{-21}	376	135	−74 434
NGC 6218	4.8	-9^{+3}_{-9}	135^{+6}_{-10}	158^{+6}_{-7}	$5.0^{+0.4}_{-0.1}$	$2.3^{+0.3}_{-0.2}$	$0.37^{+0.05}_{-0.02}$	37^{+2}_{-2}	64	581	−158 135

Table 1 *Continued.*

Name	d_{GC} (kpc)	Π (km s)	Θ (km s)	$V_{\rm tot}$ (km s)	apo (kpc)	peri (kpc)	ecc	incl. θ (deg)	T_r (Myr)	L_Z (kpc km s)	E (km^2 s^{-2})
FSR 1735	4.3	-102^{+17}_{-7}	-5^{+15}_{-21}	225^{+16}_{-12}	$5.3^{+0.6}_{-0.3}$	$1.0^{+0.5}_{-0.1}$	$0.69^{+0.03}_{-0.10}$	92^{+6}_{-4}	68	−22	−157 538
NGC 6235	4.0	159^{+8}_{-5}	197^{+28}_{-40}	256^{+24}_{-30}	$6.2^{+1.2}_{-1.1}$	$2.7^{+0.4}_{-0.5}$	$0.39^{+0.05}_{-0.03}$	53^{+11}_{-7}	84	570	−145 439
NGC 6254	4.8	-87^{+4}_{-7}	134^{+13}_{-16}	167^{+9}_{-10}	$5.2^{+0.2}_{-0.3}$	$2.1^{+0.3}_{-0.4}$	$0.42^{+0.06}_{-0.06}$	36^{+4}_{-1}	78	606	−157 472
NGC 6256	2.9	-170^{+18}_{-0}	28^{+39}_{-18}	198^{+4}_{-11}	$4.4^{+0.9}_{-0.8}$	$0.1^{+0.3}_{-0.1}$	$0.94^{+0.04}_{-0.15}$	78^{+7}_{-14}	46	79	−181 873
Pal 15	38.2	154^{+9}_{-13}	-5^{+26}_{-17}	162^{+9}_{-11}	$54.6^{+2.8}_{-4.4}$	$1.2^{+3.0}_{-0.3}$	$0.96^{+0.01}_{-0.11}$	98^{+18}_{-35}	726	−165	−53 233
NGC 6266	2.0	42^{+17}_{-15}	122^{+10}_{-18}	146^{+6}_{-11}	$2.5^{+0.5}_{-0.4}$	$0.6^{+0.3}_{-0.1}$	$0.62^{+0.04}_{-0.10}$	32^{+4}_{-4}	32	215	−205 537
NGC 6273	1.6	-98^{+67}_{-143}	-240^{+218}_{-34}	315^{+8}_{-4}	$3.8^{+0.6}_{-0.3}$	$1.0^{+0.3}_{-0.1}$	$0.59^{+0.11}_{-0.08}$	109^{+10}_{-18}	48	−144	−172 941
NGC 6284	7.3	14^{+2}_{-2}	-2^{+7}_{-19}	113^{+12}_{-6}	$7.5^{+0.9}_{-0.9}$	$0.7^{+0.3}_{-0.2}$	$0.83^{+0.04}_{-0.06}$	91^{+10}_{-4}	90	−16	−142 332
NGC 6287	2.0	-301^{+264}_{-107}	-64^{+40}_{-80}	318^{+5}_{-4}	$5.3^{+0.6}_{-0.5}$	$0.8^{+0.1}_{-0.1}$	$0.75^{+0.04}_{-0.02}$	95^{+3}_{-3}	66	−60	−159 009
NGC 6293	1.8	-152^{+52}_{-33}	-80^{+115}_{-36}	233^{+7}_{-10}	$3.6^{+0.4}_{-1.0}$	$0.2^{+0.2}_{-0.1}$	$0.91^{+0.08}_{-0.17}$	131^{+7}_{-39}	38	−93	−191 358
NGC 6304	2.5	79^{+5}_{-10}	191^{+7}_{-6}	219^{+5}_{-6}	$3.3^{+0.4}_{-0.6}$	$1.8^{+0.2}_{-0.4}$	$0.29^{+0.04}_{-0.02}$	20^{+2}_{-2}	52	474	−183 132
NGC 6316	2.4	103^{+9}_{-7}	51^{+26}_{-33}	143^{+16}_{-11}	$3.0^{+0.5}_{-0.6}$	$0.4^{+0.1}_{-0.3}$	$0.77^{+0.18}_{-0.03}$	40^{+31}_{-16}	36	106	−197 316
NGC 6341	9.8	53^{+6}_{-4}	13^{+9}_{-5}	109^{+12}_{-13}	$10.7^{+0.3}_{-0.3}$	$0.3^{+0.2}_{-0.1}$	$0.94^{+0.02}_{-0.04}$	79^{+4}_{-9}	124	108	−125 312
NGC 6325	1.3	-81^{+29}_{-48}	-181^{+187}_{-63}	214^{+17}_{-19}	$1.3^{+0.4}_{-0.1}$	$1.1^{+0.2}_{-0.3}$	$0.12^{+0.16}_{-0.00}$	114^{+13}_{-25}	18	−107	−212 097
NGC 6333	1.8	-89^{+122}_{-118}	346^{+6}_{-48}	364^{+5}_{-3}	$6.4^{+0.8}_{-0.2}$	$1.0^{+0.2}_{-0.1}$	$0.74^{+0.02}_{-0.03}$	59^{+2}_{-6}	74	327	−151 409
NGC 6342	1.6	-25^{+70}_{-89}	164^{+13}_{-66}	168^{+6}_{-4}	$1.7^{+0.7}_{-0.3}$	$0.9^{+0.2}_{-0.4}$	$0.31^{+0.29}_{-0.12}$	64^{+6}_{-3}	24	117	−207 010
NGC 6356	7.2	47^{+5}_{-9}	107^{+25}_{-12}	160^{+17}_{-7}	$7.9^{+1.3}_{-1.1}$	$2.5^{+1.0}_{-0.5}$	$0.52^{+0.06}_{-0.10}$	43^{+3}_{-4}	104	713	−136 303
NGC 6355	1.2	-207^{+70}_{-47}	-110^{+108}_{-54}	275^{+8}_{-10}	$2.2^{+1.1}_{-0.5}$	$0.6^{+0.2}_{-0.2}$	$0.56^{+0.17}_{-0.10}$	106^{+8}_{-10}	28	−95	−199 192
NGC 6352	3.6	42^{+18}_{-13}	226^{+5}_{-13}	230^{+4}_{-10}	$4.1^{+0.6}_{-0.3}$	$3.2^{+0.2}_{-0.3}$	$0.13^{+0.05}_{-0.03}$	12^{+1}_{-1}	68	794	−163 864
IC 1257	17.6	-45^{+7}_{-12}	-50^{+12}_{-18}	70^{+12}_{-0}	$18.1^{+1.1}_{-0.8}$	$1.8^{+0.8}_{-0.4}$	$0.82^{+0.04}_{-0.08}$	158^{+4}_{-11}	208	−817	−98 556
Terzan 2	1.0	-120^{+62}_{-23}	-47^{+13}_{-48}	136^{+3}_{-2}	$1.2^{+0.3}_{-0.4}$	$0.1^{+0.1}_{-0.0}$	$0.86^{+0.05}_{-0.19}$	161^{+3}_{-19}	14	−44	−242 360
NGC 6366	5.3	94^{+3}_{-3}	134^{+2}_{-6}	175^{+2}_{-5}	$5.8^{+0.2}_{-0.2}$	$2.2^{+0.1}_{-0.2}$	$0.45^{+0.03}_{-0.00}$	32^{+2}_{-1}	74	699	−153 378
Terzan 4	1.2	15^{+8}_{-39}	75^{+18}_{-13}	124^{+14}_{-8}	$1.3^{+0.2}_{-0.4}$	$0.2^{+0.1}_{-0.1}$	$0.68^{+0.03}_{-0.10}$	52^{+7}_{-6}	14	92	−234 494
BH 229	0.5	7^{+46}_{-39}	-55^{+48}_{-0}	292^{+14}_{-22}	$0.8^{+1.1}_{-0.1}$	$0.3^{+0.4}_{-0.2}$	$0.49^{+0.32}_{-0.18}$	100^{+0}_{-9}	10	−21	−249 808
FSR 1758	3.7	60^{+30}_{-60}	-347^{+8}_{-6}	405^{+8}_{-8}	$14.3^{+2.3}_{-2.1}$	$3.7^{+0.4}_{-0.5}$	$0.59^{+0.03}_{-0.02}$	148^{+2}_{-2}	178	−1275	−106 508
NGC 6362	5.2	17^{+14}_{-28}	124^{+11}_{-6}	160^{+11}_{-4}	$5.3^{+0.2}_{-0.4}$	$2.5^{+0.2}_{-0.3}$	$0.37^{+0.04}_{-0.04}$	45^{+2}_{-4}	70	583	−153 468
Liller 1	0.8	107^{+25}_{-57}	-56^{+61}_{-43}	123^{+28}_{-31}	$0.8^{+0.2}_{-0.1}$	$0.1^{+0.2}_{-0.1}$	$0.81^{+0.13}_{-0.16}$	155^{+16}_{-74}	8	−42	−261 395
NGC6380	3.1	-62^{+5}_{-14}	-35^{+16}_{-9}	72^{+14}_{-7}	$3.4^{+0.2}_{-0.6}$	$0.2^{+0.1}_{-0.1}$	$0.89^{+0.05}_{-0.07}$	168^{+11}_{-26}	40	−105	−194 646
Terzan 1	1.6	-73^{+3}_{-5}	63^{+10}_{-20}	96^{+8}_{-11}	$1.8^{+0.5}_{-0.6}$	$0.2^{+0.1}_{-0.1}$	$0.79^{+0.06}_{-0.04}$	11^{+10}_{-6}	22	102	−224 803
Pismis 26	1.4	-112^{+111}_{-58}	204^{+32}_{-55}	307^{+9}_{-8}	$3.2^{+0.8}_{-0.1}$	$0.9^{+0.7}_{-0.4}$	$0.56^{+0.17}_{-0.20}$	41^{+9}_{-2}	44	271	−186 876
NGC 6388	3.0	-66^{+24}_{-19}	-94^{+18}_{-12}	116^{+6}_{-7}	$3.5^{+0.4}_{-0.2}$	$0.7^{+0.4}_{-0.2}$	$0.69^{+0.07}_{-0.13}$	148^{+8}_{-9}	46	−257	−190 150
NGC 6402	4.0	-20^{+23}_{-21}	48^{+10}_{-7}	57^{+16}_{-7}	$4.8^{+0.2}_{-0.5}$	$0.3^{+0.2}_{-0.0}$	$0.88^{+0.00}_{-0.08}$	47^{+6}_{-10}	52	158	−176 457
NGC 6401	2.5	-30^{+27}_{-18}	-254^{+4}_{-4}	302^{+8}_{-4}	$4.5^{+0.8}_{-0.7}$	$2.4^{+0.6}_{-0.6}$	$0.31^{+0.07}_{-0.03}$	143^{+2}_{-3}	62	−595	−161 761
NGC 6397	6.3	35^{+7}_{-6}	127^{+11}_{-6}	179^{+9}_{-4}	$6.5^{+0.1}_{-0.2}$	$2.8^{+0.3}_{-0.2}$	$0.40^{+0.03}_{-0.04}$	43^{+2}_{-4}	86	796	−144 538
Pal 6	2.5	-191^{+2}_{-3}	21^{+16}_{-14}	246^{+6}_{-8}	$4.5^{+0.4}_{-0.8}$	$0.1^{+0.1}_{-0.0}$	$0.96^{+0.01}_{-0.03}$	83^{+4}_{-6}	44	52	−179 351
NGC 6426	14.3	-112^{+27}_{-16}	93^{+7}_{-20}	148^{+11}_{-25}	$16.6^{+1.1}_{-0.7}$	$3.2^{+0.5}_{-0.9}$	$0.67^{+0.08}_{-0.03}$	27^{+4}_{-4}	202	1216	−100 666
Djorg 1	1.2	-252^{+271}_{-102}	315^{+49}_{-51}	404^{+12}_{-9}	$5.9^{+1.6}_{-1.6}$	$0.8^{+0.1}_{-0.2}$	$0.76^{+0.05}_{-0.06}$	21^{+13}_{-7}	66	351	−161 437
Terzan 5	1.5	84^{+11}_{-6}	70^{+13}_{-23}	114^{+9}_{-7}	$1.7^{+0.5}_{-0.6}$	$0.2^{+0.1}_{-0.1}$	$0.78^{+0.04}_{-0.05}$	33^{+18}_{-7}	20	104	−226 313
NGC 6440	1.3	91^{+18}_{-36}	-42^{+54}_{-34}	107^{+10}_{-8}	$1.4^{+0.4}_{-0.0}$	$0.2^{+0.1}_{-0.1}$	$0.78^{+0.15}_{-0.07}$	116^{+21}_{-34}	14	−49	−231 796
NGC 6441	3.6	16^{+15}_{-8}	66^{+18}_{-19}	71^{+20}_{-16}	$3.6^{+0.7}_{-0.6}$	$0.8^{+0.2}_{-0.2}$	$0.66^{+0.09}_{-0.07}$	21^{+11}_{-6}	42	228	−186 312
Terzan 6	1.5	-138^{+7}_{-3}	-51^{+21}_{-32}	153^{+9}_{-3}	$2.0^{+0.2}_{-0.6}$	$0.1^{+0.1}_{-0.1}$	$0.86^{+0.05}_{-0.11}$	157^{+17}_{-26}	22	−77	−220 185
NGC 6453	3.4	-105^{+9}_{-6}	38^{+30}_{-15}	194^{+19}_{-5}	$3.9^{+0.8}_{-0.6}$	$0.9^{+0.5}_{-0.1}$	$0.61^{+0.04}_{-0.14}$	78^{+5}_{-8}	54	129	−172 906
NGC 6496	4.0	-37^{+76}_{-63}	320^{+24}_{-41}	328^{+26}_{-28}	$9.1^{+2.1}_{-1.6}$	$3.7^{+0.4}_{-0.6}$	$0.42^{+0.10}_{-0.07}$	32^{+5}_{-3}	120	1111	−126 509
Terzan 9	1.3	-50^{+8}_{-7}	22^{+18}_{-14}	76^{+7}_{-2}	$1.4^{+0.6}_{-0.4}$	$0.1^{+0.1}_{-0.0}$	$0.92^{+0.03}_{-0.08}$	70^{+12}_{-13}	16	29	−236 057
Djorg 2	2.0	161^{+9}_{-6}	155^{+6}_{-11}	228^{+3}_{-4}	$3.2^{+0.6}_{-0.7}$	$0.9^{+0.3}_{-0.3}$	$0.57^{+0.06}_{-0.04}$	11^{+1}_{-1}	42	316	−192 751
NGC 6517	4.0	55^{+8}_{-17}	33^{+10}_{-12}	73^{+5}_{-11}	$4.6^{+0.4}_{-0.4}$	$0.2^{+0.1}_{-0.1}$	$0.91^{+0.03}_{-0.04}$	58^{+10}_{-10}	50	127	−179 281
Terzan 10	2.2	231^{+20}_{-52}	87^{+64}_{-22}	343^{+20}_{-13}	$5.9^{+1.4}_{-1.8}$	$0.7^{+0.3}_{-0.1}$	$0.79^{+0.04}_{-0.11}$	72^{+4}_{-10}	76	193	−155 422
NGC 6522	0.8	34^{+25}_{-15}	92^{+23}_{-57}	213^{+17}_{-9}	$1.2^{+0.5}_{-0.3}$	$0.2^{+0.3}_{-0.2}$	$0.67^{+0.14}_{-0.15}$	63^{+16}_{-6}	16	58	−238 519
NGC 6535	4.0	93^{+9}_{-10}	-83^{+13}_{-6}	133^{+2}_{-6}	$4.6^{+0.4}_{-0.3}$	$1.0^{+0.1}_{-0.2}$	$0.64^{+0.06}_{-0.03}$	160^{+1}_{-3}	56	−320	−173 024
NGC 6528	0.7	-197^{+300}_{-67}	113^{+31}_{-67}	229^{+2}_{-2}	$1.0^{+0.9}_{-0.2}$	$0.3^{+0.0}_{-0.2}$	$0.60^{+0.33}_{-0.14}$	70^{+7}_{-5}	14	51	−241 883
NGC 6539	3.1	1^{+28}_{-9}	118^{+5}_{-3}	208^{+14}_{-9}	$3.4^{+0.3}_{-0.2}$	$1.9^{+0.2}_{-0.3}$	$0.30^{+0.08}_{-0.03}$	56^{+1}_{-2}	56	347	−174 387
NGC 6540	3.0	13^{+3}_{-2}	148^{+9}_{-7}	159^{+8}_{-5}	$3.1^{+0.4}_{-0.4}$	$1.6^{+0.3}_{-0.2}$	$0.32^{+0.04}_{-0.04}$	22^{+2}_{-1}	48	448	−187 517
NGC 6544	5.3	6^{+2}_{-2}	6^{+14}_{-10}	91^{+8}_{-7}	$5.6^{+0.2}_{-0.1}$	$0.1^{+0.2}_{-0.0}$	$0.98^{+0.00}_{-0.06}$	86^{+7}_{-9}	52	31	−166 630
NGC 6541	2.3	123^{+33}_{-62}	192^{+25}_{-20}	254^{+11}_{-6}	$3.8^{+0.6}_{-0.6}$	$1.3^{+0.2}_{-0.1}$	$0.50^{+0.08}_{-0.10}$	40^{+6}_{-4}	50	334	−174 968
ESO 280-06	13.8	31^{+5}_{-10}	16^{+10}_{-25}	91^{+8}_{-11}	$14.2^{+1.1}_{-1.3}$	$0.9^{+0.5}_{-0.4}$	$0.88^{+0.05}_{-0.05}$	77^{+20}_{-7}	164	210	−109 791
NGC 6553	2.4	45^{+15}_{-12}	245^{+2}_{-4}	250^{+2}_{-3}	$3.3^{+0.3}_{-0.4}$	$2.3^{+0.4}_{-0.5}$	$0.19^{+0.04}_{-0.04}$	7^{+2}_{-1}	52	588	−179 839
NGC 6558	1.2	187^{+60}_{-94}	93^{+36}_{-60}	209^{+4}_{-4}	$1.7^{+0.4}_{-0.6}$	$0.3^{+0.2}_{-0.0}$	$0.72^{+0.08}_{-0.29}$	63^{+15}_{-8}	20	87	−217 130

Table 1 *Continued.*

Name	d_{GC} (kpc)	Π (km s)	Θ (km s)	$V_{\rm tot}$ (km s)	apo (kpc)	peri (kpc)	ecc	incl. θ (deg)	T_r (Myr)	L_Z (kpc km s)	E (km^2 s^{-2})
Pal 7	3.9	-74^{+12}_{-9}	270^{+7}_{-4}	281^{+7}_{-4}	$6.0^{+0.6}_{-0.4}$	$3.5^{+0.3}_{-0.1}$	$0.26^{+0.02}_{-0.02}$	11^{+1}_{-1}	86	1042	−147 032
Terzan 12	3.6	-94^{+5}_{-4}	172^{+8}_{-9}	219^{+6}_{-6}	$4.4^{+0.4}_{-0.5}$	$2.2^{+0.2}_{-0.3}$	$0.33^{+0.04}_{-0.03}$	28^{+2}_{-2}	62	625	−167 749
NGC 6569	2.8	-40^{+2}_{-4}	174^{+18}_{-26}	180^{+18}_{-25}	$3.0^{+0.6}_{-0.7}$	$1.9^{+0.3}_{-0.7}$	$0.23^{+0.17}_{-0.05}$	26^{+12}_{-5}	56	440	−182 361
ESO 456-78	2.0	71^{+10}_{-10}	199^{+5}_{-4}	252^{+7}_{-6}	$2.9^{+0.6}_{-0.2}$	$1.4^{+0.5}_{-0.3}$	$0.34^{+0.06}_{-0.07}$	34^{+2}_{-2}	52	373	−186 632
NGC 6584	6.8	197^{+7}_{-30}	98^{+22}_{-34}	324^{+11}_{-22}	$18.0^{+2.1}_{-2.8}$	$1.7^{+0.7}_{-0.6}$	$0.83^{+0.05}_{-0.06}$	52^{+12}_{-3}	212	556	−98 089
NGC 6624	1.2	-29^{+48}_{-24}	60^{+14}_{-18}	136^{+7}_{-4}	$1.5^{+0.3}_{-0.0}$	$0.2^{+0.1}_{-0.2}$	$0.78^{+0.18}_{-0.05}$	73^{+3}_{-6}	20	37	−226 410
NGC 6626	3.0	-28^{+2}_{-4}	57^{+9}_{-12}	113^{+8}_{-5}	$3.1^{+0.5}_{-0.1}$	$0.5^{+0.1}_{-0.2}$	$0.75^{+0.10}_{-0.04}$	60^{+6}_{-4}	42	169	−193 067
NGC 6638	2.0	68^{+16}_{-12}	14^{+13}_{-21}	74^{+14}_{-7}	$2.4^{+0.5}_{-0.1}$	$0.1^{+0.0}_{-0.0}$	$0.95^{+0.03}_{-0.03}$	80^{+16}_{-9}	20	22	−212 068
NGC 6637	1.6	35^{+27}_{-111}	91^{+6}_{-81}	129^{+8}_{-8}	$2.2^{+0.2}_{-0.4}$	$0.2^{+0.0}_{-0.1}$	$0.87^{+0.11}_{-0.01}$	77^{+17}_{-5}	22	40	−212 500
NGC 6642	1.7	112^{+6}_{-22}	25^{+32}_{-51}	125^{+8}_{-11}	$2.2^{+0.3}_{-0.1}$	$0.1^{+0.2}_{-0.0}$	$0.94^{+0.02}_{-0.11}$	46^{+78}_{-17}	24	36	−215 457
NGC 6652	2.5	-54^{+6}_{-4}	28^{+7}_{-18}	186^{+11}_{-16}	$4.2^{+0.2}_{-0.3}$	$0.1^{+0.1}_{-0.1}$	$0.96^{+0.03}_{-0.05}$	76^{+9}_{-5}	38	42	−183 595
NGC 6656	5.2	176^{+3}_{-2}	201^{+2}_{-2}	303^{+6}_{-5}	$9.8^{+0.7}_{-0.5}$	$3.1^{+0.2}_{-0.1}$	$0.53^{+0.01}_{-0.01}$	33^{+2}_{-2}	126	1044	−125 471
Pal 8	5.3	-21^{+13}_{-25}	117^{+23}_{-15}	122^{+27}_{-15}	$5.6^{+0.3}_{-0.6}$	$1.8^{+0.6}_{-0.4}$	$0.51^{+0.06}_{-0.11}$	23^{+3}_{-2}	72	593	−160 020
NGC 6681	2.0	221^{+34}_{-166}	55^{+135}_{-44}	287^{+9}_{-3}	$4.5^{+0.3}_{-0.4}$	$0.7^{+0.5}_{-0.1}$	$0.74^{+0.10}_{-0.15}$	84^{+8}_{-9}	52	36	−167 768
NGC 6712	3.6	146^{+6}_{-7}	26^{+9}_{-17}	208^{+7}_{-10}	$5.5^{+0.3}_{-0.2}$	$0.2^{+0.1}_{-0.1}$	$0.93^{+0.04}_{-0.02}$	78^{+7}_{-4}	56	93	−168 544
NGC 6715	18.6	232^{+6}_{-8}	49^{+25}_{-22}	317^{+21}_{-11}	$56.4^{+24.2}_{-10.1}$	$14.8^{+1.8}_{-1.0}$	$0.58^{+0.07}_{-0.03}$	81^{+4}_{-4}	906	850	−48 159
NGC 6717	2.5	-10^{+31}_{-13}	116^{+8}_{-9}	119^{+9}_{-7}	$2.8^{+0.4}_{-0.4}$	$0.7^{+0.2}_{-0.1}$	$0.59^{+0.06}_{-0.09}$	32^{+7}_{-4}	36	251	−195 762
NGC 6723	2.6	100^{+6}_{-192}	-178^{+353}_{-3}	208^{+5}_{-5}	$3.1^{+0.4}_{-0.0}$	$1.8^{+0.2}_{-0.0}$	$0.26^{+0.05}_{-0.03}$	90^{+8}_{-12}	40	−2	−175 356
NGC 6749	5.0	-23^{+17}_{-10}	110^{+10}_{-9}	112^{+10}_{-8}	$5.1^{+0.4}_{-0.2}$	$1.6^{+0.2}_{-0.1}$	$0.53^{+0.05}_{-0.05}$	3^{+1}_{-0}	62	556	−167 068
NGC 6752	5.5	-23^{+7}_{-2}	179^{+3}_{-6}	190^{+3}_{-6}	$5.7^{+0.3}_{-0.3}$	$3.6^{+0.2}_{-0.2}$	$0.23^{+0.02}_{-0.02}$	24^{+1}_{-0}	82	931	−147 164
NGC 6760	5.0	92^{+10}_{-9}	147^{+7}_{-8}	174^{+7}_{-7}	$5.6^{+0.3}_{-0.3}$	$2.2^{+0.2}_{-0.2}$	$0.44^{+0.04}_{-0.03}$	6^{+1}_{-0}	72	724	−158 732
NGC 6779	9.3	155^{+3}_{-2}	-15^{+6}_{-9}	185^{+6}_{-4}	$12.4^{+0.4}_{-0.6}$	$0.3^{+0.2}_{-0.1}$	$0.96^{+0.01}_{-0.03}$	101^{+7}_{-5}	134	−135	−119 696
Terzan 7	15.3	260^{+6}_{-6}	25^{+17}_{-11}	320^{+11}_{-11}	$42.9^{+7.7}_{-8.3}$	$12.8^{+0.6}_{-1.1}$	$0.54^{+0.05}_{-0.05}$	86^{+2}_{-3}	668	335	−56 545
Pal 10	6.6	-56^{+15}_{-5}	186^{+8}_{-13}	195^{+7}_{-14}	$7.0^{+0.3}_{-0.3}$	$4.0^{+0.4}_{-0.4}$	$0.27^{+0.04}_{-0.03}$	8^{+1}_{-1}	100	1234	−138 495
Arp 2	21.2	243^{+7}_{-8}	68^{+20}_{-11}	311^{+10}_{-15}	$65.1^{+21.7}_{-13.5}$	$17.8^{+1.7}_{-1.6}$	$0.57^{+0.06}_{-0.04}$	78^{+2}_{-4}	1094	1256	−43 628
NGC 6809	4.1	-199^{+5}_{-7}	76^{+15}_{-19}	220^{+5}_{-3}	$5.7^{+0.4}_{-0.5}$	$1.2^{+0.3}_{-0.3}$	$0.66^{+0.06}_{-0.07}$	67^{+6}_{-3}	76	266	−154 417
Terzan 8	19.1	269^{+8}_{-5}	37^{+16}_{-23}	315^{+12}_{-7}	$58.5^{+13.5}_{-6.8}$	$16.0^{+0.8}_{-0.8}$	$0.57^{+0.06}_{-0.03}$	84^{+4}_{-3}	958	584	−46 785
Pal 11	8.1	-16^{+28}_{-20}	139^{+12}_{-10}	140^{+14}_{-9}	$8.2^{+0.7}_{-0.4}$	$3.5^{+0.6}_{-0.4}$	$0.40^{+0.05}_{-0.04}$	27^{+3}_{-2}	108	1013	−132 057
NGC 6838	7.0	39^{+5}_{-11}	204^{+5}_{-4}	212^{+4}_{-4}	$7.3^{+0.2}_{-0.2}$	$5.0^{+0.3}_{-0.2}$	$0.18^{+0.02}_{-0.03}$	12^{+1}_{-1}	112	1423	−132 307
NGC 6864	14.6	-99^{+14}_{-6}	18^{+10}_{-25}	111^{+7}_{-14}	$16.4^{+1.3}_{-0.4}$	$0.5^{+0.6}_{-0.5}$	$0.94^{+0.06}_{-0.05}$	61^{+41}_{-9}	186	209	−103 615
NGC 6934	12.7	-289^{+20}_{-18}	103^{+20}_{-30}	330^{+15}_{-17}	$40.9^{+7.8}_{-5.8}$	$2.5^{+0.6}_{-0.8}$	$0.88^{+0.04}_{-0.03}$	23^{+5}_{-2}	520	1204	−63 341
NGC 6981	12.8	-154^{+10}_{-13}	-4^{+14}_{-25}	230^{+10}_{-7}	$22.3^{+2.1}_{-1.3}$	$0.3^{+0.3}_{-0.1}$	$0.97^{+0.01}_{-0.03}$	108^{+25}_{-36}	252	−35	−89 722
NGC 7006	38.5	-140^{+6}_{-8}	-33^{+17}_{-7}	168^{+9}_{-12}	$56.3^{+2.3}_{-4.5}$	$2.9^{+0.7}_{-1.5}$	$0.90^{+0.05}_{-0.02}$	133^{+13}_{-13}	760	−1170	−52 073
NGC 7078	10.6	8^{+11}_{-12}	118^{+8}_{-11}	122^{+9}_{-10}	$10.6^{+0.5}_{-0.5}$	$3.5^{+0.4}_{-0.5}$	$0.50^{+0.05}_{-0.04}$	28^{+3}_{-1}	140	1119	−119 947
NGC 7089	10.4	170^{+5}_{-6}	-18^{+12}_{-15}	243^{+8}_{-8}	$18.8^{+1.7}_{-1.0}$	$0.6^{+0.2}_{-0.3}$	$0.94^{+0.03}_{-0.02}$	119^{+12}_{-20}	214	−147	−97 640
NGC 7099	7.2	-32^{+14}_{-9}	-55^{+16}_{-12}	126^{+8}_{-9}	$8.2^{+0.6}_{-0.5}$	$1.0^{+0.3}_{-0.3}$	$0.78^{+0.06}_{-0.05}$	119^{+3}_{-6}	94	−234	−137 480
Pal 12	15.7	146^{+22}_{-37}	304^{+22}_{-24}	356^{+12}_{-17}	$72.0^{+18.9}_{-16.0}$	$15.5^{+1.0}_{-0.9}$	$0.65^{+0.05}_{-0.08}$	67^{+2}_{-2}	1178	2142	−41 826
Pal 13	27.0	268^{+6}_{-11}	-78^{+21}_{-17}	289^{+9}_{-12}	$87.1^{+8.6}_{-13.4}$	$8.3^{+0.9}_{-1.9}$	$0.83^{+0.03}_{-0.02}$	115^{+8}_{-6}	1346	−1586	−38 661
NGC 7492	25.4	-87^{+16}_{-22}	-13^{+9}_{-7}	108^{+19}_{-10}	$28.2^{+2.5}_{-2.3}$	$3.1^{+1.4}_{-1.0}$	$0.80^{+0.06}_{-0.07}$	95^{+6}_{-5}	352	−120	−77 041

parameters. Comparison of the most important orbital parameters ($E, L_Z, ecc, L_Z/ecc, V_{\rm tot}, Apo, \theta, T_r$) is given in Figure 1. In this figure the parameters obtained for the GCs with the distances, which are both larger by 7% and less by 7% than the nominal ones, are compared with the corresponding orbital parameters obtained for the GCs with nominal distances.

It should be especially noted that among the analyzed parameters we also included the ratio L_Z/ecc, the bimodality of the distribution of which we used in Bajkova et al. (2020) to separate GCs belonging to the thick disk and halo. The influence of the uncertainty in the GC distances of 7% led to a standard deviation of this ratio of 5% (relative to effective range of this parameter), which we expect did not affect the result of GC classification due to the high stability of the separation algorithm reported in the work Bajkova et al. (2020). The greatest influence from uncertainty in distances of 7% is experienced by such parameters as eccentricity (ecc) and inclination of orbit θ. The standard deviations of these parameters are 7.6 and 8.4%, respectively. All other parameters are significantly less influenced, with a standard deviation of not larger than 3% in each case.

5 ORBITS OF 152 GLOBULAR CLUSTERS AND THEIR PROPERTIES

The orbits of the 152 GCs were obtained by integrating Equation (7) for 5 Gyr backward. The (X, Y) and (R, Z)

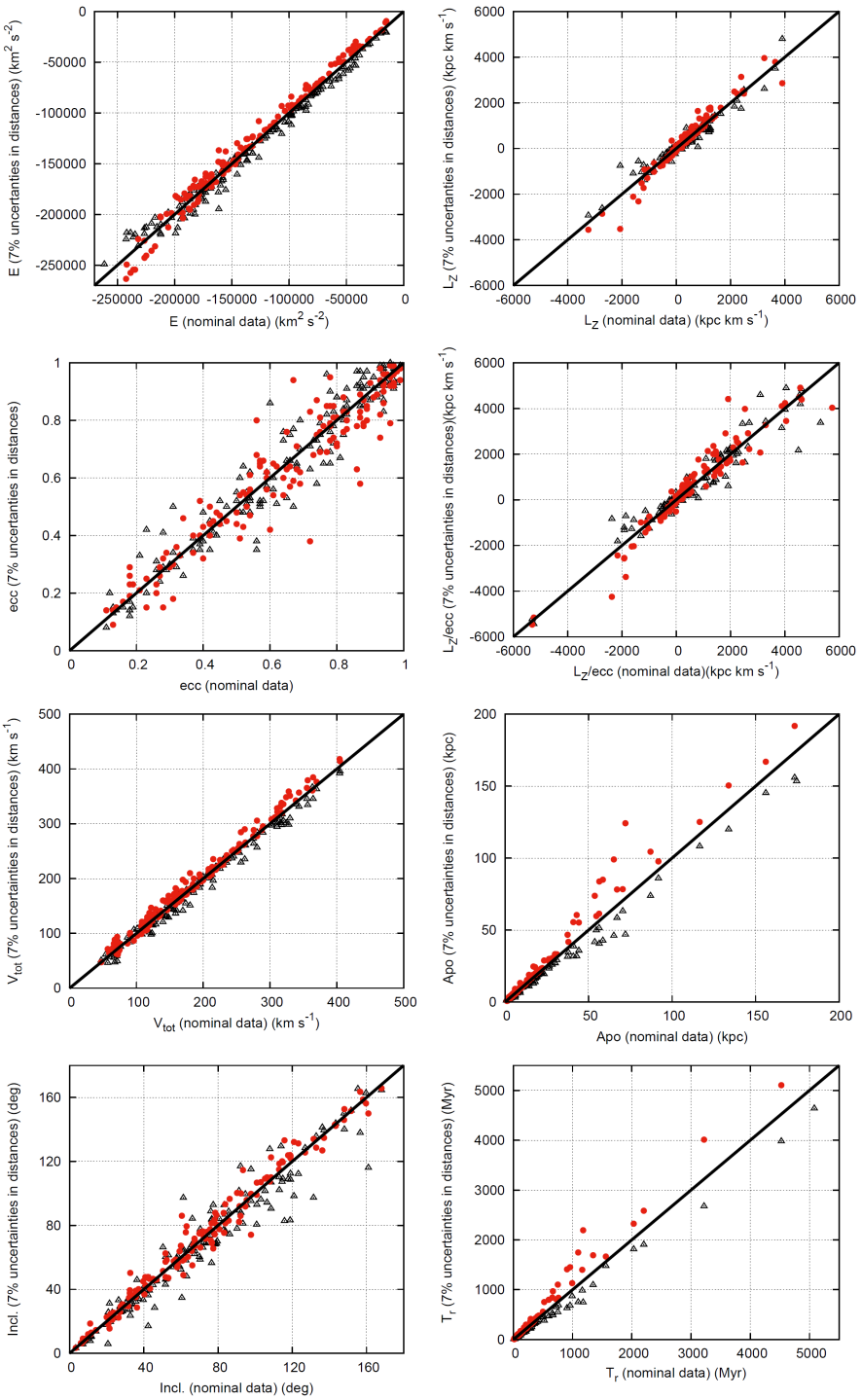

Fig. 1 Comparison of the GCs' orbital parameters ($E, L_Z, ecc, L_Z/ecc, V_{\rm tot}, Apo, \theta, T_r$). The parameters obtained for the GCs, with distances which are larger by 7% (*red points*) and less by 7% (*black triangles*) than the nominal ones, are compared with the corresponding orbital parameters obtained for the GCs with nominal distances.

orbit projections for each of the GCs are presented in Figure 2. The orbital properties are presented in Table 1. To calculate the uncertainties in the orbital properties, we applied the Monte Carlo method with 100 realizations, taking into account the uncertainties in the initial coordinates and velocities of GCs, as well as errors in the peculiar velocity of the Sun. For parameters T_r, L_Z and E, we only give nominal values in Table 1 to save space.

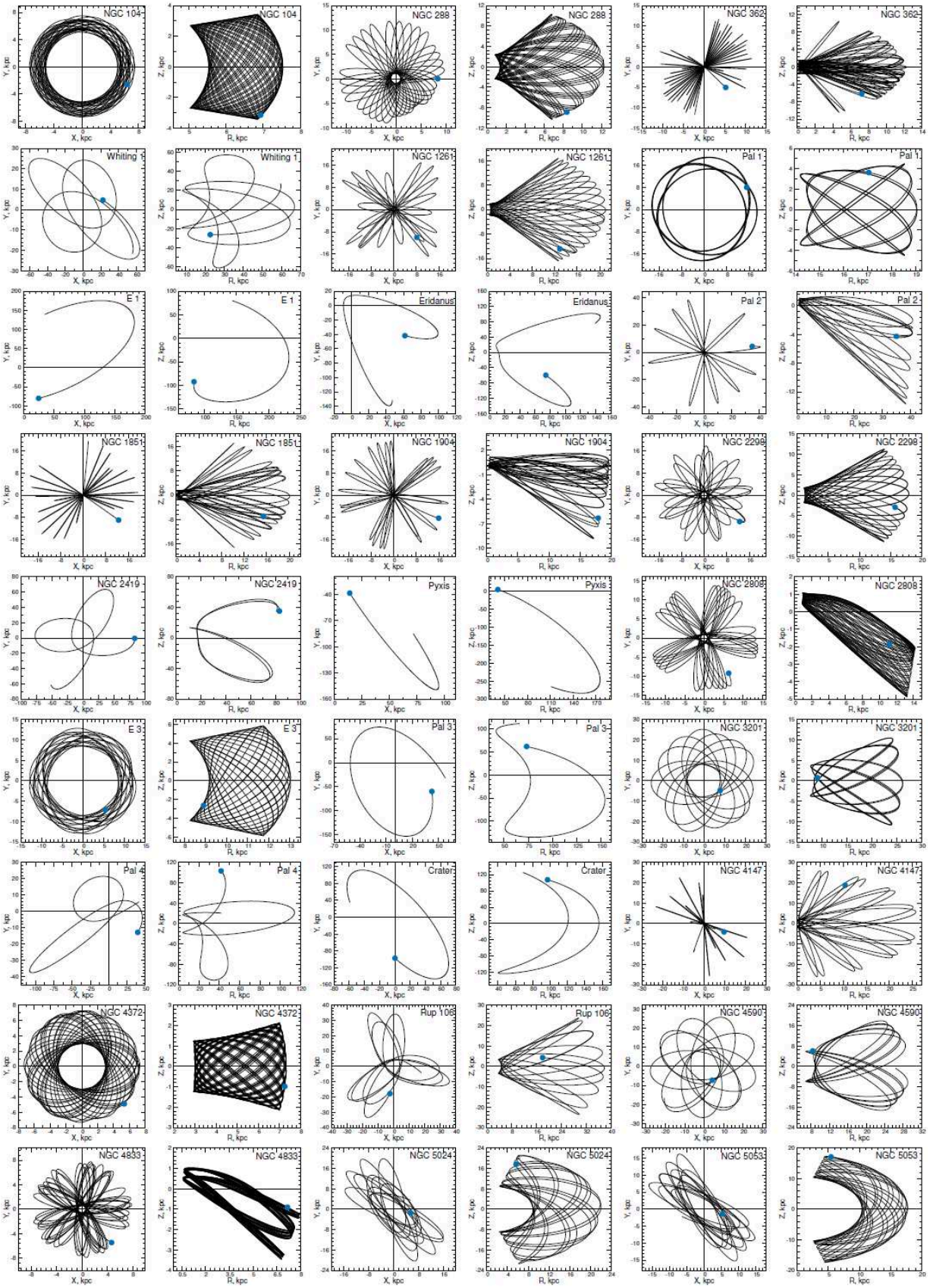

Fig. 2 Orbits of the GCs obtained by integrating 5 Gyr backward. (X, Y) and (R, Z) projections are given. The *blue filled circle* indicates the beginning of the orbit.

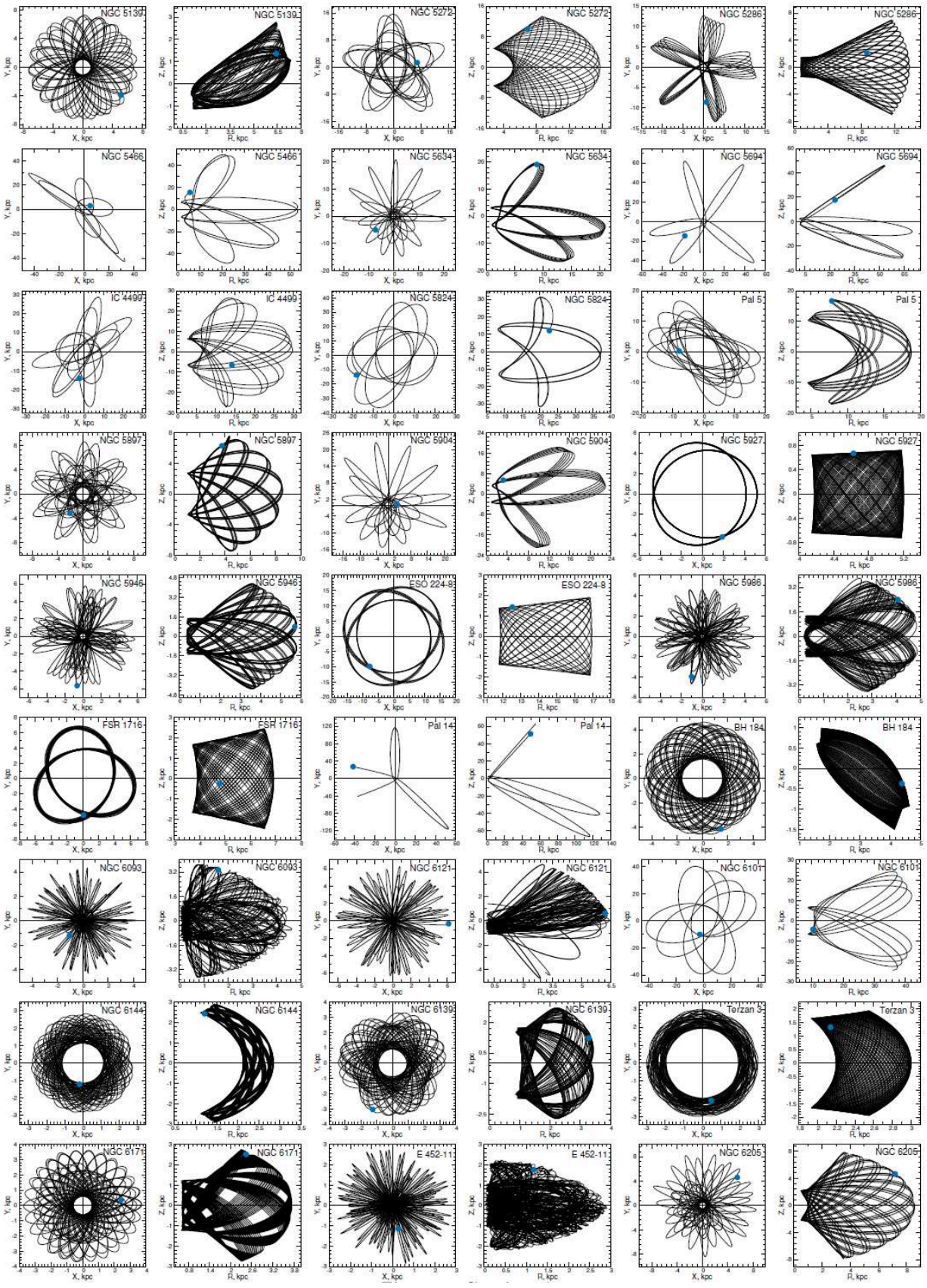

Fig. 2 *Continued.*

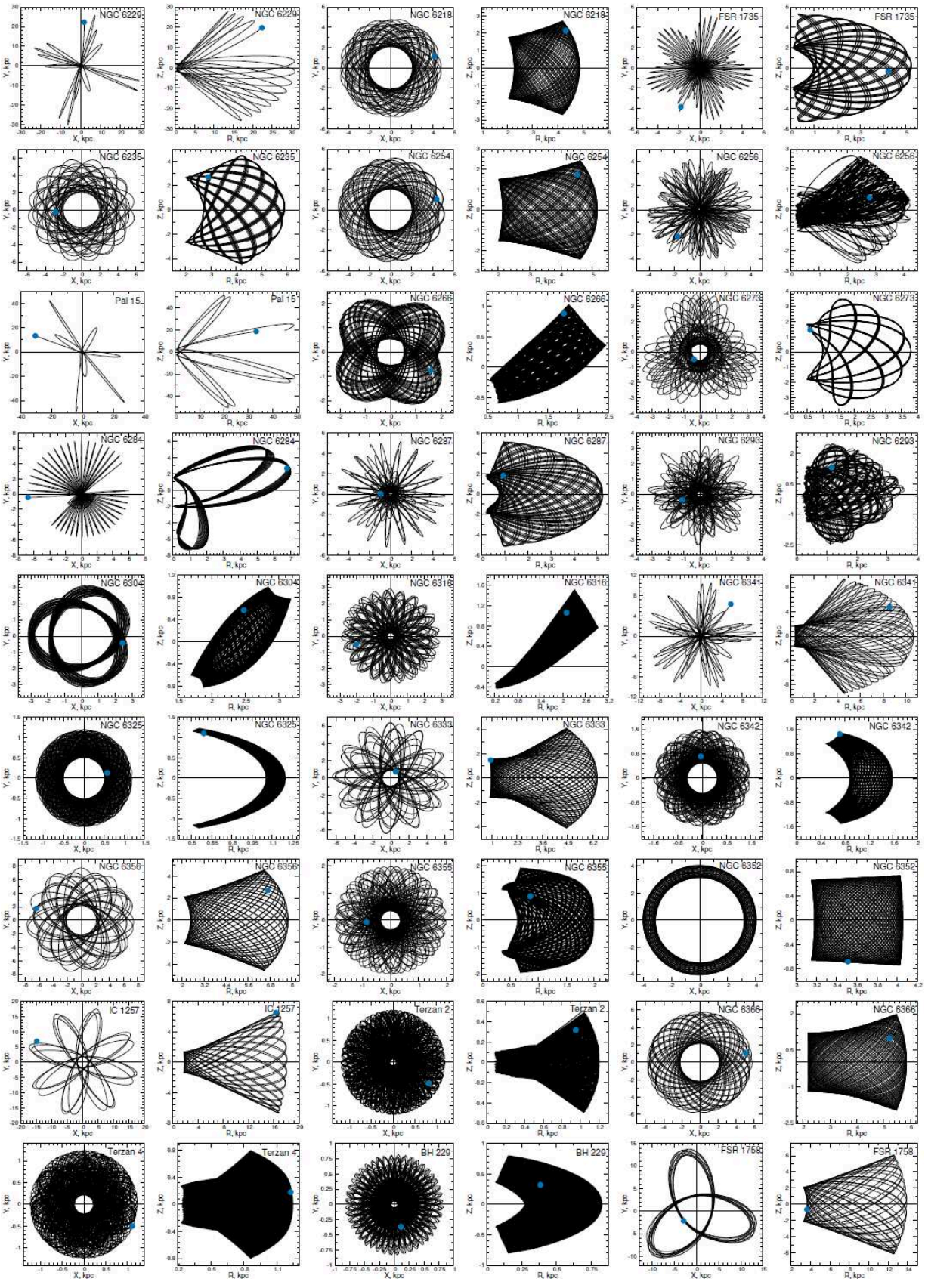

Fig. 2 *Continued.*

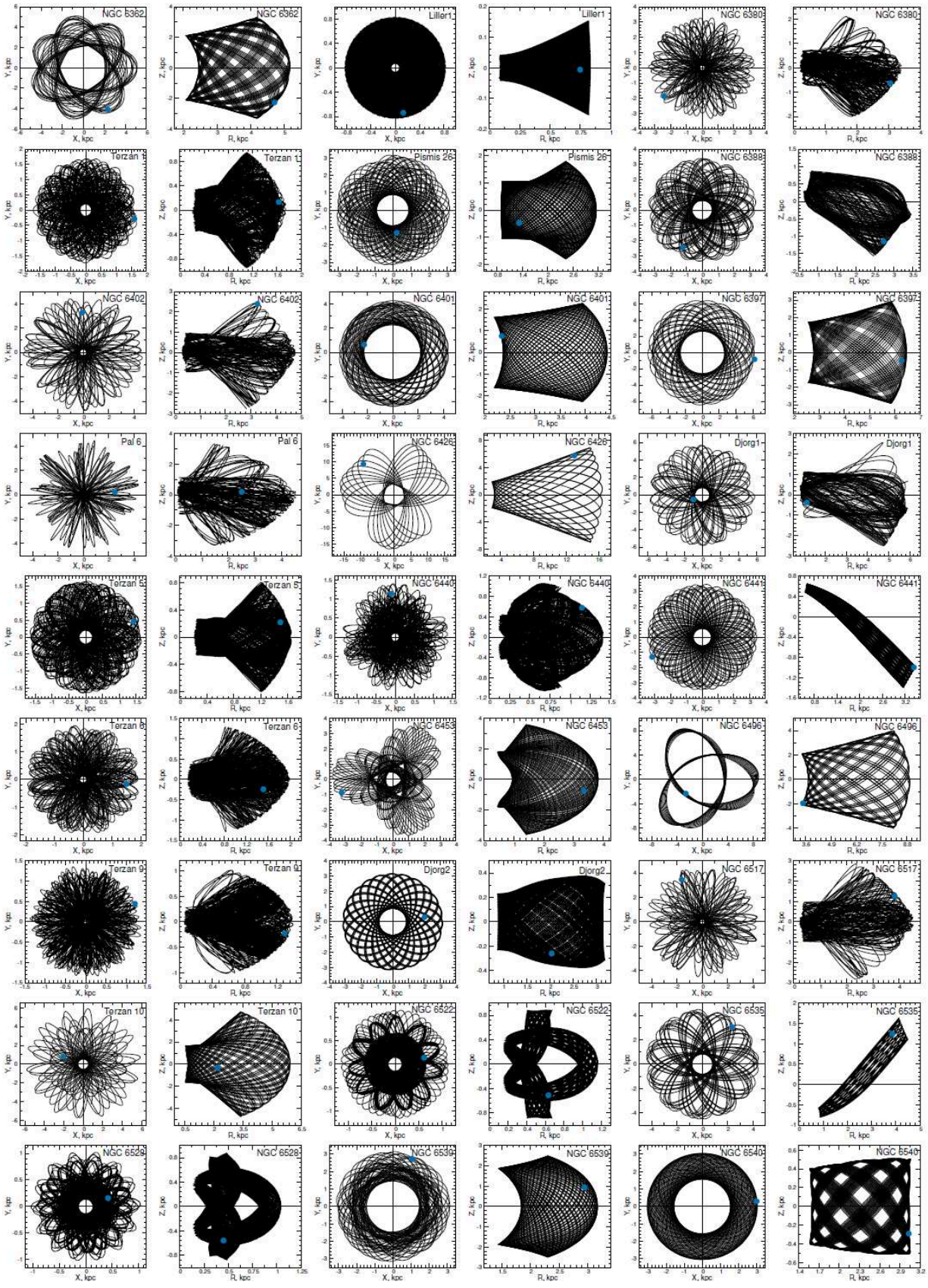

Fig. 2 *Continued.*

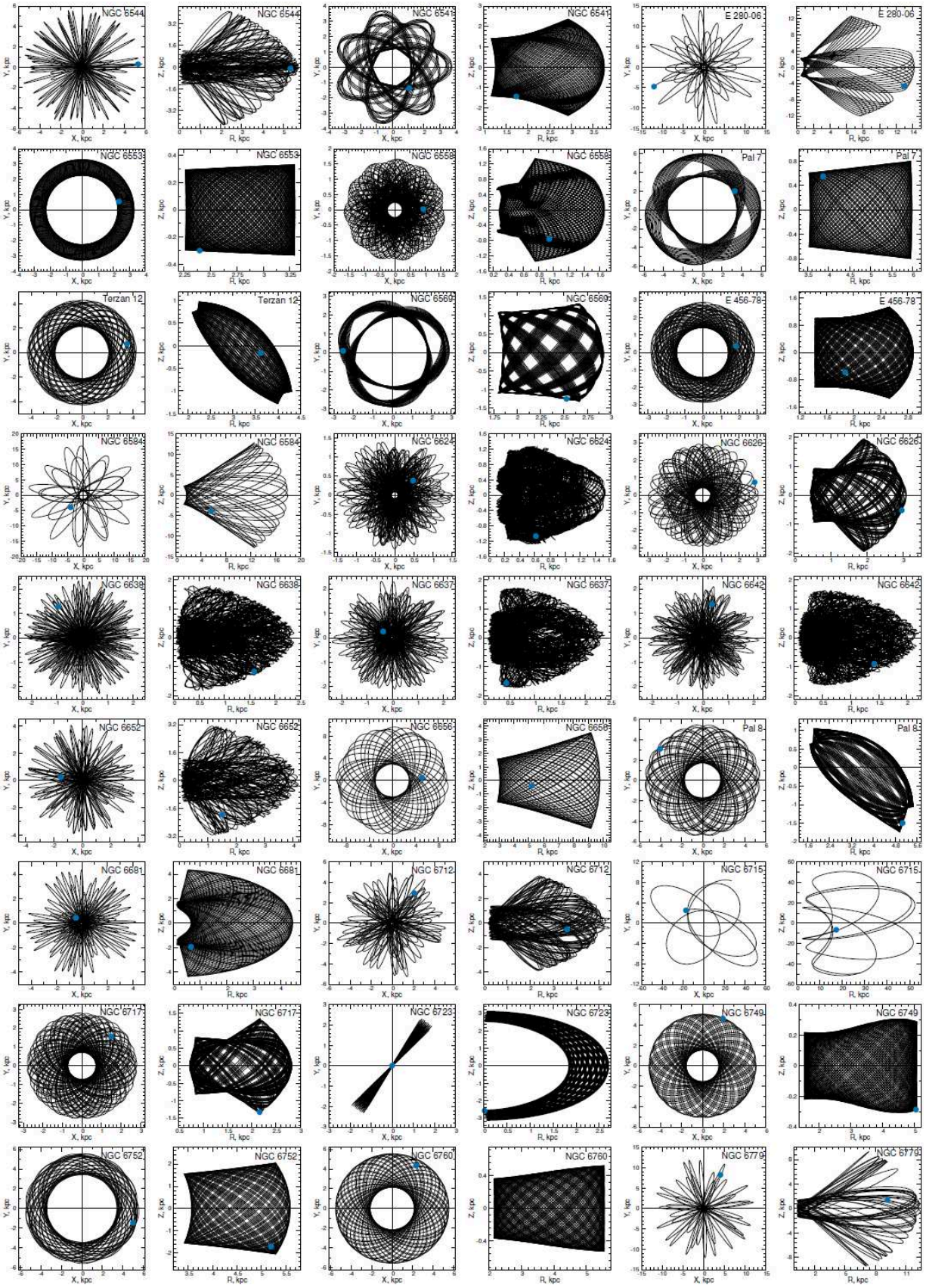

Fig. 2 *Continued.*

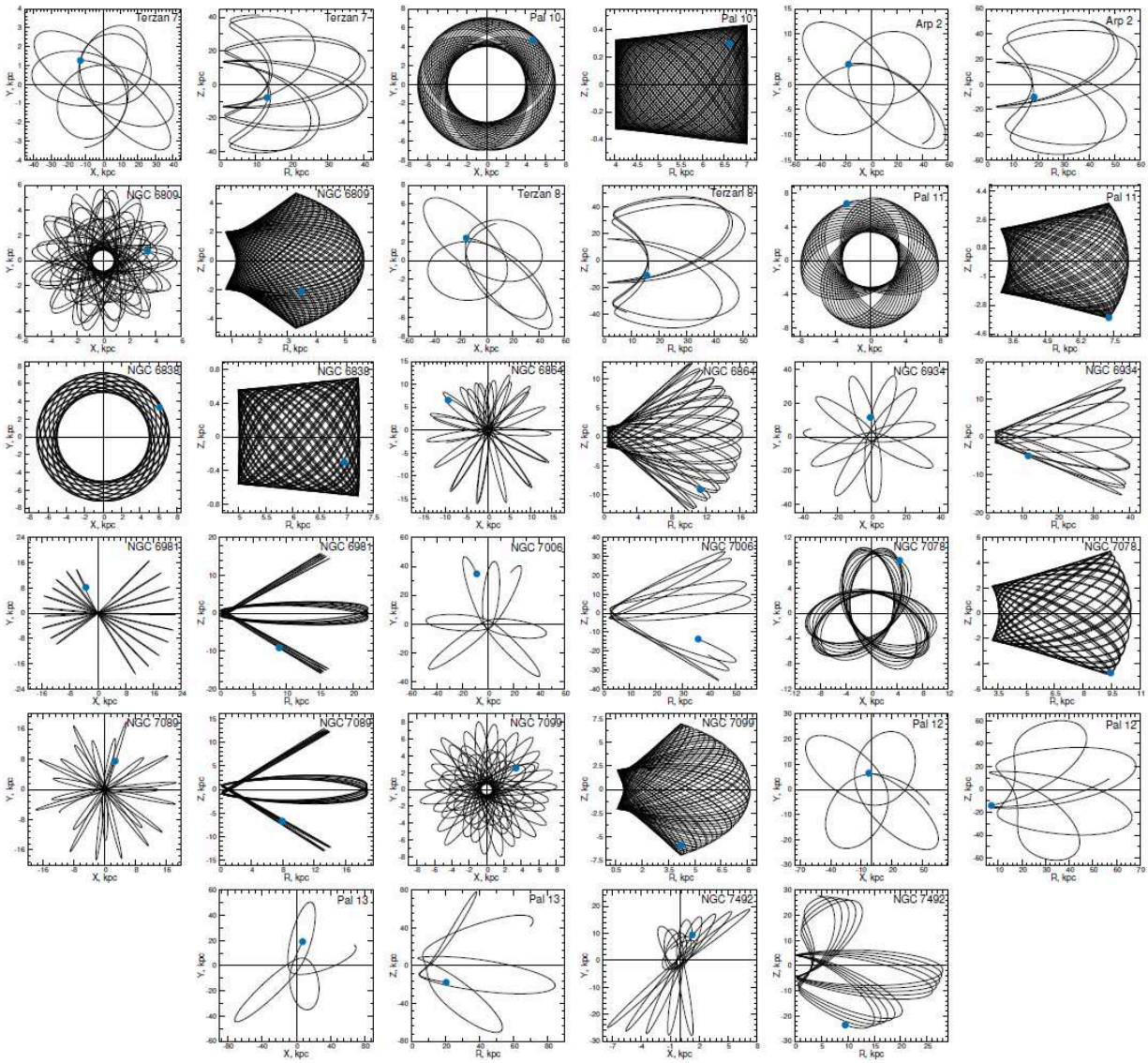

Fig. 2 *Continued.*

Table 2 GCs with Modified Classification

Name	GS	GS(m)	Name	GS	GS(m)	Name	GS	GS(m)
E 3	H99	D	NGC 6254	LE	D	NGC 6553	B	D
NGC 5466	Seq	GE	NGC 6304	B	D	NGC 6569	B	D
NGC 5634	H99	GE	Liller 1	XXX	B	ESO 456-78	B	D
NGC 5694	HE	GE	NGC 6388	B	Seq	NGC 6584	HE	GE
NGC 5824	Sgr	H99	NGC 6401	LE	Seq	NGC 6712	LE	GE
NGC 5904	H99	GE	NGC 6426	HE	H99	NGC 6934	HE	GE
Pal 14	HE	GE	NGC 6539	B	D	NGC 6981	H99	GE
NGC 6144	LE	Seq	NGC 6540	B	D	NGC 7006	Seq	GE
NGC 6235	GE	D	NGC 6544	LE	GE	Pal 13	Seq	GE

Based on the analysis of orbits and their properties, a small regrouping of GCs by subsystems has been made. Table 2 shows 27 GCs, which have changed their group membership to one group or another. In this table, the column designated as GS – Galactic Subsystem, gives the classification proposed by Massari et al. (2019), and the column designated as GS(m), lists a modified classification. The following designations for the Galactic subsystems are used here: D (disk), B (bulge), GE (Gaia-Enceladus, or Gaia-Sausage), H99 (Helmi

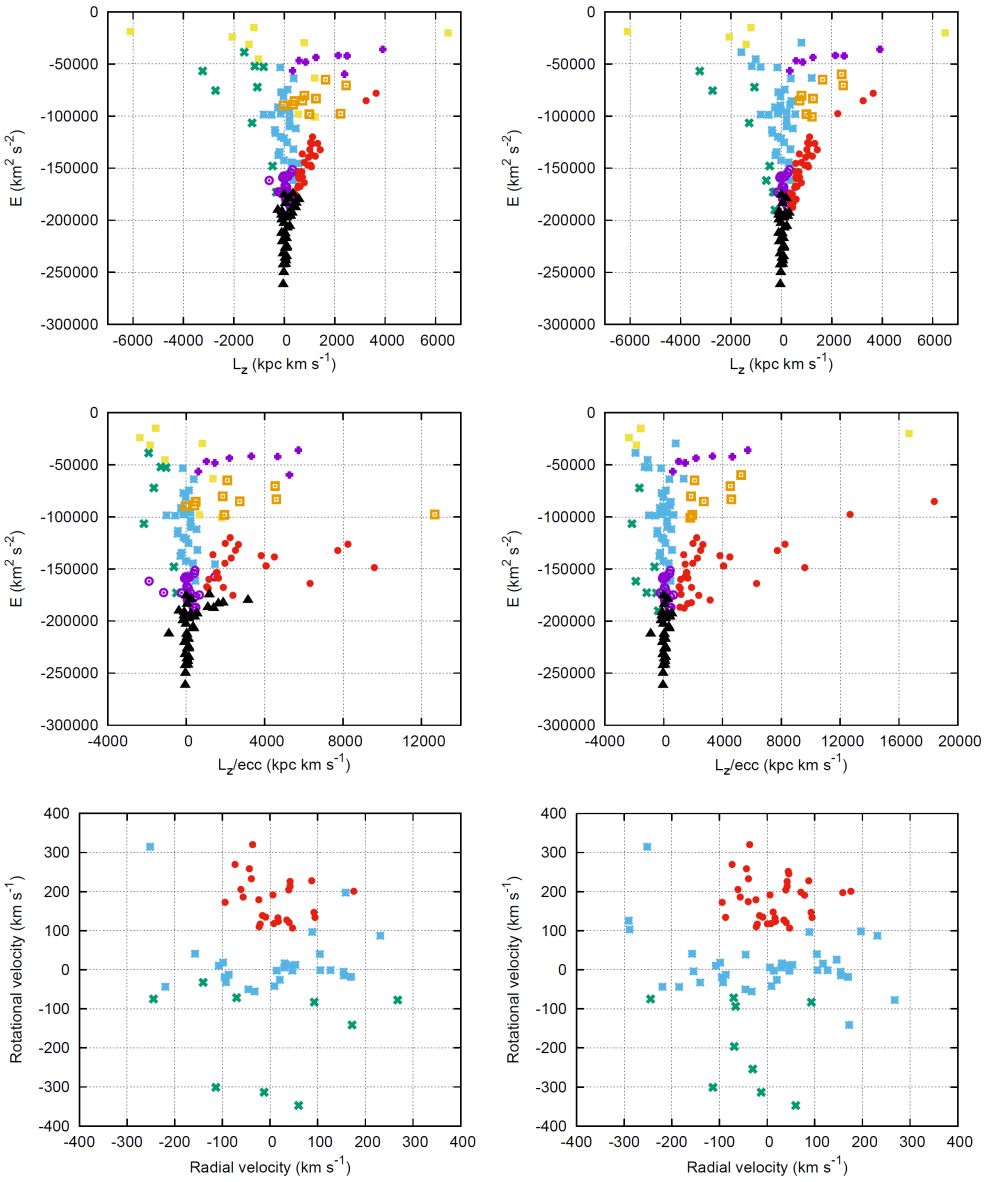

Fig. 3 The "L_Z – Energy" (*top panels*), "L_Z/ecc – Energy" (*middle panels*) and "Radial velocity – Rotational velocity" (*bottom panels*) diagrams for GCs. Classification by Massari et al. (2019) (*left-hand panels*); the modified classification (*right-hand panels*). They are color-coded according to their belonging to different subsystems (*red symbols* mark the disk, *black* is for the bulge, *blue* is for Gaia-Enceladus (Gaia-Sausage), *orange* for Helmi Streams, *green* for Sequoia, *violet crosses* for Sagittarius, *yellow* for the high-energy group and *violet circles* for the low-energy group. For visualization purposes, cluster E 1 with extremely negative L_Z has not been plotted.

Streams), Seq (Sequoia galaxy), Sgr (Sagittarius dwarf), HE (unassociated High-Energy), LE (unassociated Low-Energy) and XXX (clusters with no available kinematics).

The separation of GCs into subsystems of the bulge/bar, thick disk and halo was performed by us in Bajkova et al. (2020) applying a criterion based on the bimodal distribution of GCs over parameter L_Z/ecc. The composition of the bulge/bar and thick disk reflects these results. In the redistribution of the remaining GCs between the halo subsystems (GE, Seq, Sgr, H99), we took into account the parameters of the orbits. For example, GCs with strong radially elongated orbits were assigned to GE. The rest of the rearrangement also took into account the proximity of the orbital shapes.

In Figure 3 the "L_Z– Energy", "L_Z/ecc– Energy" and "Radial velocity – Rotational velocity" diagrams are presented. These diagrams are provided both for classification of GCs by Massari et al. (2019) and for

the modified one for comparison. As you can see from Figure 2, the modified classification looks like a more correct one from the point of view of a greater similarity of the orbits of GCs included in their subsystem. From a comparison of the diagrams "L_Z – Energy", "L_Z/ecc – Energy" and "Radial velocity – Rotational velocity", it can also be concluded that the modified classification is more organic.

6 CONCLUSIONS

For the first time since the publication of the Gaia DR2, a catalog of orbits for 152 Galactic GCs, which form an almost complete known population, is presented.

The main orbital parameters of GCs are determined. The astrometric data catalog compiled by Vasiliev (2019) was used as data for calculating the initial 6D phase space (heliocentric positions and velocities of GCs) needed for orbit construction. The orbits were integrated 5 Gyr backward.

For integrating the orbits, we relied on the best-fit model of an axisymmetric Galactic potential recently obtained by Bajkova & Bobylev (2016), with a dark halo in the form of NFW (Navarro et al. 1997) using data on circular velocities of Galactic objects in a wide range of galactocentric distances (data on HI region, masers and catalog of Bhattacharjee et al. 2014).

Based on the analysis of the obtained orbits and their properties, we have formed a modified composition of the subsystems of GCs, slightly different from the composition presented in Massari et al. (2019). This modification affected 27 GCs. The modified classification looks like a more correct one from the point of view of a greater similarity of the orbits of GCs included in their subsystem.

Acknowledgements The authors would like to express gratitude to the anonymous referee for useful remarks, the consideration of which made it possible to significantly improve the article. The authors are also grateful to Dr. Dambis A.K. for useful discussion.

References

Bajkova, A. T., & Bobylev, V. V. 2016, Astronomy Letters, 42, 567
Bajkova, A. T., & Bobylev, V. V. 2017, Open Astronomy, 26, 72
Bajkova, A. T., Carraro, G., Korchagin, V. I., Budanova, N. O., & Bobylev, V. V. 2020, ApJ, 895, 69
Baumgardt, H., Hilker, M., Sollima, A., & Bellini, A. 2019, MNRAS, 482, 5138
Bhattacharjee, P., Chaudhury, S., & Kundu, S. 2014, ApJ, 785, 63
Bobylev, V. V., & Bajkova, A. T. 2016, Astronomy Letters, 42, 1
Harris, W. 2010, arXiv: 1012.3224
Gaia Collaboration, Helmi, A., van Leeuwen, F., et al. 2018, A&A, 616, 12
Irrgang, A., Wilcox, B., Tucker, E., & Schiefelbein, L. 2013, A&A, 549, 137
Koppelman, H. H., & Helmi, A. 2020, arXiv: 2006.16283
Massari, D., Koppelman, H. H., & Helmi, A. 2019, A&A, 630, L4
Miyamoto, M., & Nagai, R. 1975, PASJ, 27, 533
Myeong, G. C., Vasiliev, E., Iorio, G., Evans, N. W., & Belokurov, V. 2019, MNRAS, 488, 1235
Navarro, J. F., Frenk, C. S., & White, S. D. M. 1997, ApJ, 490, 493
Schonrich, R., Binney, J.. & Dehnen, W. 2010, MNRAS, 403, 1829
Vasiliev, E. 2018, arXiv: 1807.09775v1
Vasiliev, E. 2019, MNRAS, 484, 2832
Villanova, S., Monaco, L., Geisler, D., et al. 2019, ApJ, 882, 174